JOURNAL OF MATERIALS SCIENCE 9 (1974) 1467–1477

The deformation behaviour of a dispersion strengthened superplastic zinc alloy

J. D. LEE*, P. NIESSEN
Department of Mechanical Engineering, University of Waterloo, Waterloo, Ontario, Canada

The deformation behaviour of a new dispersion strengthened superplastic zinc alloy was investigated. A significant long range internal stress was observed at all strain-rates. The activation volume of deformation decreased very rapidly with a decrease in the true effective stress. The maximum strain-rate sensitivity corresponds to a region of change from this high stress dependence of the activation volume to a much lower stress dependence. The observation of a metallographic halo effect shows that apart from dislocation movement, diffusive creep plays a role during superplastic deformation. It is stipulated that both these processes aid boundary sliding which accounts for the largest part of the strain.

1. Introduction

In an earlier paper [1] we reported on a new superplastic zinc alloy containing only 0.1 wt % Ni and 0.04 wt % Mg. This alloy exhibits a strain-rate sensitivity (m) and elongation-to-fracture as high as the Zn–22 % Al (eutectoid) alloy. However, the superplastic flow stress of this alloy is higher than that of the Zn–Al eutectoid. This new zinc alloy has a very small and stable grain size at superplastic forming temperatures due to a dispersion of Ni_3Zn_{22} and Mg_2Zn_{11} particles. This dispersion is produced through high rate continuous casting, which causes a super-saturation in Ni and Mg, and subsequent hot-working leading to precipitation and simultaneous recrystallization to form the required small grain size.

The true stress/strain-rate curve for the alloy [1] has a sigmoidal form with a maximum slope of 0.51 when presented in a double logarithmic plot. An equation of the form

$$\sigma = A'''\bar{d}^2 \exp(13.1 \times 10^3/RT)\dot{\epsilon}^{\eta+m} \qquad (1)$$

described the deformation behaviour of the alloy within the region of increasing m. In this equation A''' is a constant, R is the gas constant, σ is the true stress, $\dot{\epsilon}$ the true strain-rate, T the absolute temperature and $\bar{d}$ the average grain diameter. Of the remaining terms, m is the strain-rate sensitivity as defined in [1], and η is a constant independent of grain size but weakly dependent on temperature over the region 100 to 250° C.

The activation energy of deformation (13.1 kcal g^{-1} at.$^{-1}$) suggested that diffusive processes underlie the deformation mechanism of this alloy. However, the dependence of the flow stress on the grain size and strain-rate in Equation 1 does suggest that during the deformation of this alloy other mechanisms besides diffusion play a role. For this reason more experiments were carried out to gain an understanding of the deformation mechanism of this alloy. In particular, it was felt that long range internal stress measurements, activation volume determinations and further microstructural observations would contribute to this understanding.

2. Experimental procedures and results

All tensile testing was done on a floor model Instron fitted with a push-button speed selector and an Instron environmental chamber. The long term temperature stability of this chamber was ± 2° C, and temperature differences over the 25 cm test zone were less than ± 1° C. The round tensile specimens used had a 6 mm gauge section diameter and a gauge section length of 25 mm. Different grain sizes were obtained in this alloy by extruding the super-saturated cast billets at different temperatures [1]. The recrystallized grain diameter was determined either directly on an optical microscope employing an oil immer-

*Present address: Bell Northern Research, Ottawa, Ontario, Canada.

sion lens and Nomarski interference contrast, or from photomicrographs taken on the scanning electron microscope. The grain size determined on the optical microscope was obtained from mean linear intercept measurements on randomly oriented test lines involving more than 320 boundary intercept counts. The grain diameter was determined from the photomicrographs by randomly applying a test circle to a series of prints and counting the number of boundary intersections with the test circle in the manner outlined by Hilliard [2]. More than 100 grain intercepts were counted by this technique. Hilliard estimates a standard deviation of less than 7% for the grain diameter of reasonably equiaxed grains when more than 80 grains are counted. In the following the mean linear intercept values obtained by these two techniques are called the mean grain diameter $\bar{d}$. The grain sizes and testing temperatures employed are given in the test results which follow.

2.1. Determination of the long range internal stress

A convenient method, due to Gibbs [3], for determining the long range internal stresses is illustrated in Fig. 1. A specimen is deformed at a constant rate until a steady-state load is reached. The cross-head of the tensile machine is then rapidly reversed, decreasing the load to some value greater than zero. As shown in Fig. 1, the resultant load-time curve may exhibit two distinctly different forms. If after partial unloading the stress on the specimen is above its long range internal stress, load decay will occur. If the stress is less than the long range internal stress, negative creep occurs and the load

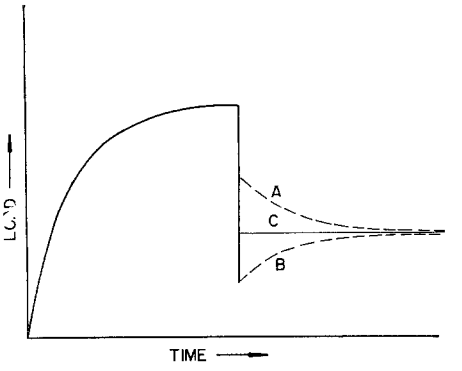

Figure 1 Method for determining the long range internal stress from a load decay chart. A – stress > long range internal stress, B – stress < long range internal stress, C – stress = long range internal stress.

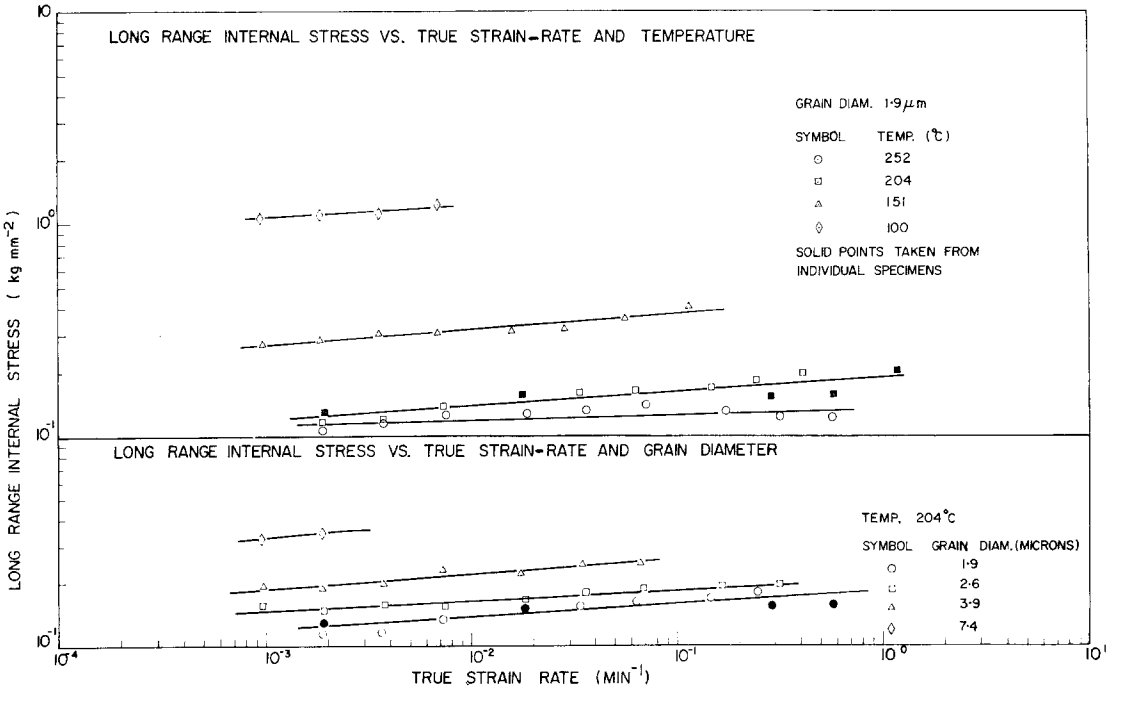

Figure 2 The variation of the long range internal stress with temperature, strain-rate and grain size.

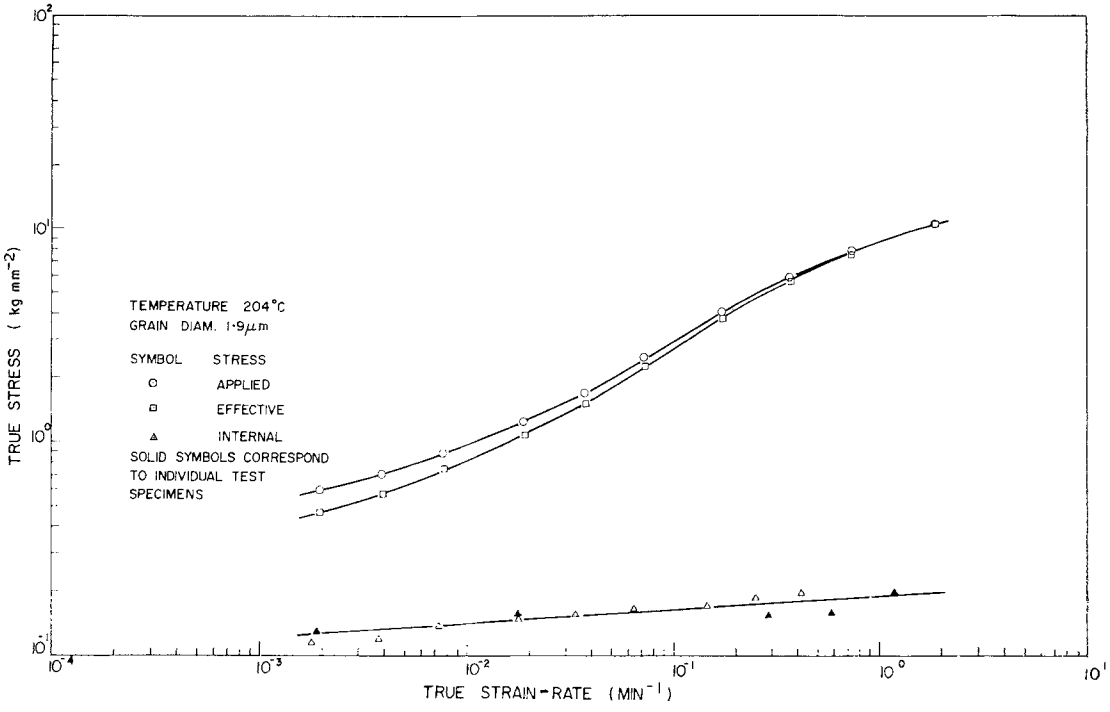

Figure 3 The variation of the applied, effective and internal stress with strain-rate.

increases with time. This load will approach the load from the positive decay curve and both values will remain constant for a short period. By incrementally removing the load, a point of constant load can be found which identifies the long range internal stress within the specimen. Because of the high recovery rate of superplastic alloys, it was more expedient for the present work to decrease the load to a value slightly less than the load corresponding to the long range internal stress. The internal stress was then determined from the steady state portion of the negative creep curve. This technique gave well defined constant loads for a period of 1 to 2 min. Repeated tests at increasing strain-rates were performed on the same specimen as well as single tests on individual specimens.

The dependence of the long range internal stress on the strain-rate for different temperatures and grain sizes is shown in Fig. 2. In this figure the lines represent the least squares fit of the data.

It is now possible to define an effective stress, σ_e, as the difference between the applied stress and the long range internal stress, σ_i, namely:

$$\sigma_e = \sigma - \sigma_i \,. \tag{2}$$

Fig. 3 shows the variation of these three stresses with strain-rate for one temperature and grain size. In general it was found that at the lower strain rate σ_i was between 20 and 35% of the applied stress.

Experiments were performed to show that the negative creep behaviour was not just a spurious effect arising out of the test system. A rigid steel specimen was loaded at 200°C to the highest load applied during testing of the zinc alloy. Negative creep was not observed on decreasing the load to the range corresponding to the internal stress of the superplastic alloy.

2.2. Determination of the activation volume

The average activation volume for high temperature deformation is generally defined as the average area, $\bar{A}$, swept out by a dislocation during a thermally activated movement, multiplied by the Burgers vector, $\boldsymbol{b}$, of the dislocation. From thermodynamic considerations [3], the average activation volume is given by

$$\bar{V} = \boldsymbol{b}\bar{A} = \frac{kT}{N}\left(\frac{\partial \ln \dot{\epsilon}}{\partial \sigma_e}\right)_T \tag{3}$$

where N is the Taylor factor, taken to be 0.5, and k is the Boltzmann constant. Equation 3 does not invoke any particular form of activation barrier and is therefore completely general. The

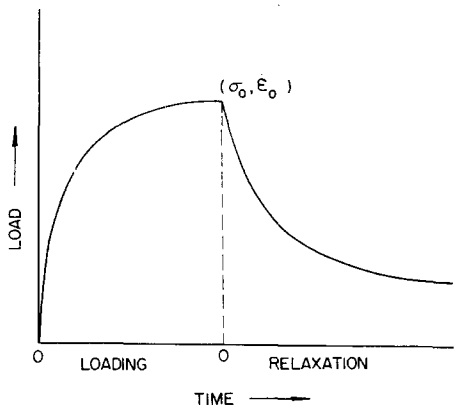

Figure 4 Schematic illustration of a load relaxation curve at stress σ_0 and strain-rate $\dot{\epsilon}_0$.

effective stress is used to signify the stress acting on a dislocation during an activation event.

The experimental average activation volume was determined by a stress relaxation technique used by Gibbs [3]. In this method a specimen is deformed at a constant temperature and rate in a hard tensile machine until a steady-state stress is reached. The machine cross-head is then arrested. Subsequent stress relaxation will occur by plastic flow of the specimen, relieving elastic strains in the machine. A typical stress relaxation curve is shown in Fig. 4. This stress-time curve has a slope which is proportional to the instantaneous creep rate.

If the stress from a load relaxation curve is plotted against the logarithm of time, a linear relationship with slope α is obtained over part of the stress range as illustrated in Fig. 5. It has been shown by Guiu and Pratt [5], that on theoretical grounds the positive value of the slope α is given by

$$\alpha = \frac{Nd\sigma_e}{d\ln \dot{\epsilon}}. \tag{4}$$

It is unlikely that the activation volume determined by this technique represents the exact activation volume at the time the cross-head stopped. However, the activation volume determined should be proportional to the true activation volume over the experimental range of strain-rates since the linear portion of the stress-log time plot consistently appeared within the time interval 0.01 to 0.05 min after stopping the cross-head.

The activation volume was also determined at the slowest strain-rates by the instantaneous increase in strain-rate technique [3]. Strain-rate ratios of 100 and larger were used in this method. Large activation volumes similar to those reported here were also obtained by this technique.

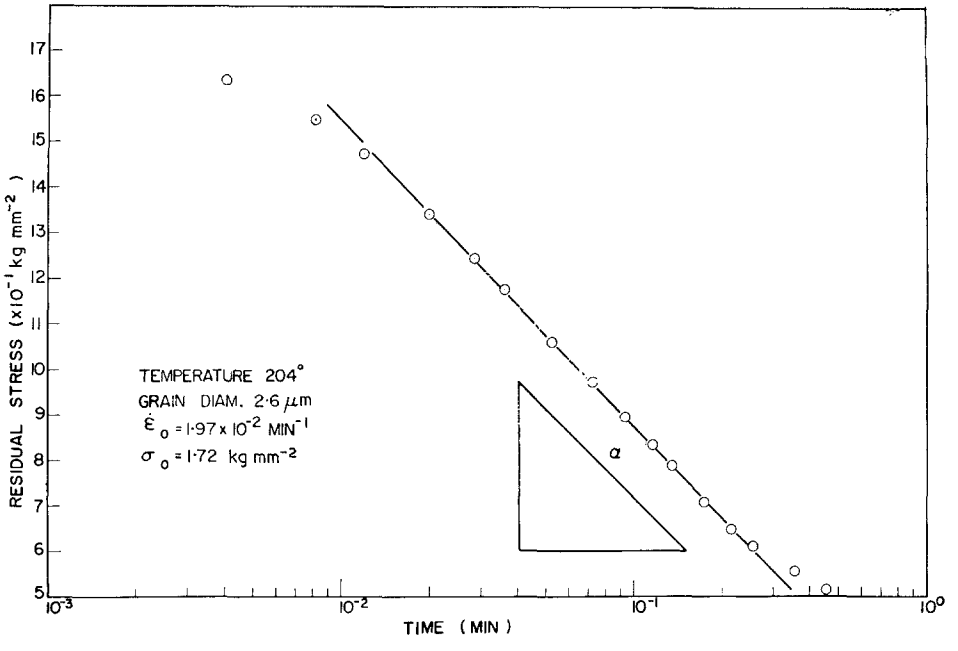

Figure 5 Semi-logarithmic plot of the residual stress versus time illustrating the method of obtaining the slope α.

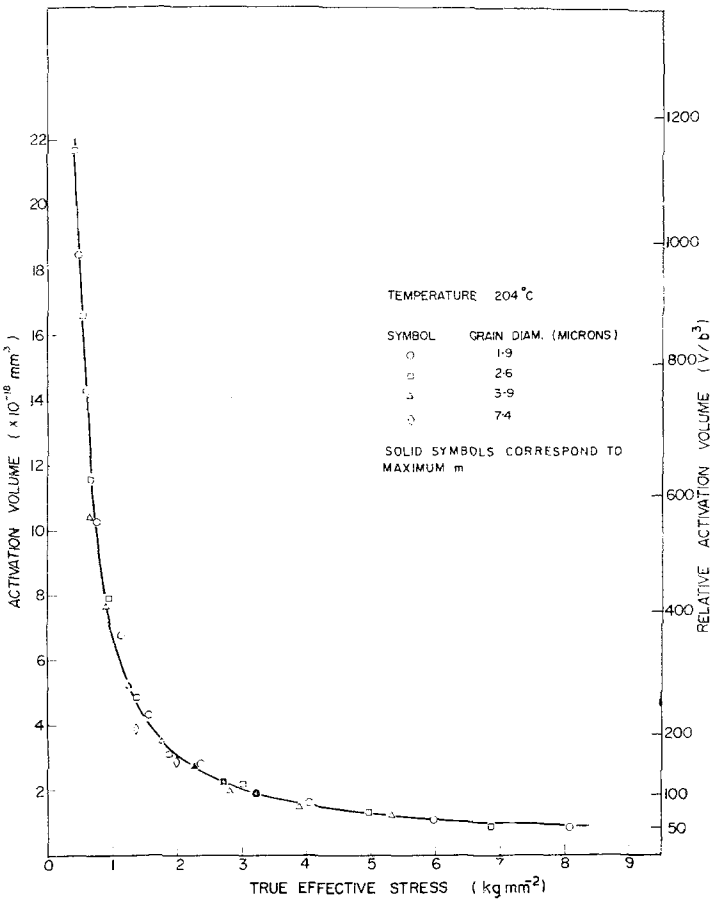

Figure 6 The true effective stress and temperature dependence of the activation volume for a grain diameter of 1.9 μm.

Like other researchers investigating elevated temperature deformation [6], we had to assume that the change of mobile dislocation density with strain-rate at the instant when $d\ln \dot{\epsilon}/d\sigma_e$ is determined is small compared with the change of stress with strain in order for Equation 3 to adequately represent the activation volume. From the measurement of α, the average activation volume was determined using

$$\bar{V} = \frac{2.3\,kT}{\alpha} \cdot \qquad (5)$$

The stress and temperature dependence of $\bar{V}$ are shown in Fig. 6. The stress and grain size dependence of $\bar{V}$ are shown in Fig. 7. The curves of Figs. 6 and 7 are identical and can be superimposed to give one line on a single graph.

2.3. Microstructural observations after superplastic deformation

Specimens for metallographic examination were strained 100% at 204°C and immediately quenched in water. Strain-rates from below to above maximum m were used. Because the strain-rate changes by a factor of 2 over a strain of 100%, the mean strain-rate $\dot{\epsilon}_m$ (at 50% strain) was used as a representative value for the entire strain.

The effect of strain-rate on the internal microstructure, i.e. in sections taken from the centre of specimens, is shown in Figs. 8 and 9. It appears that the grains have surrounded themselves with a deep etching halo which is largest in the tensile direction. This halo effect decreases as the strain-rate increases (Fig. 9).

The grain elongation is also strain dependent. Fig. 10 illustrates the technique [7] used to calculate the strain due to grain elongation. 640 grain boundaries were counted to obtain the grain length, L, and width, W. The extruded undeformed specimens had grains of slightly elongated shape which corresponded to an

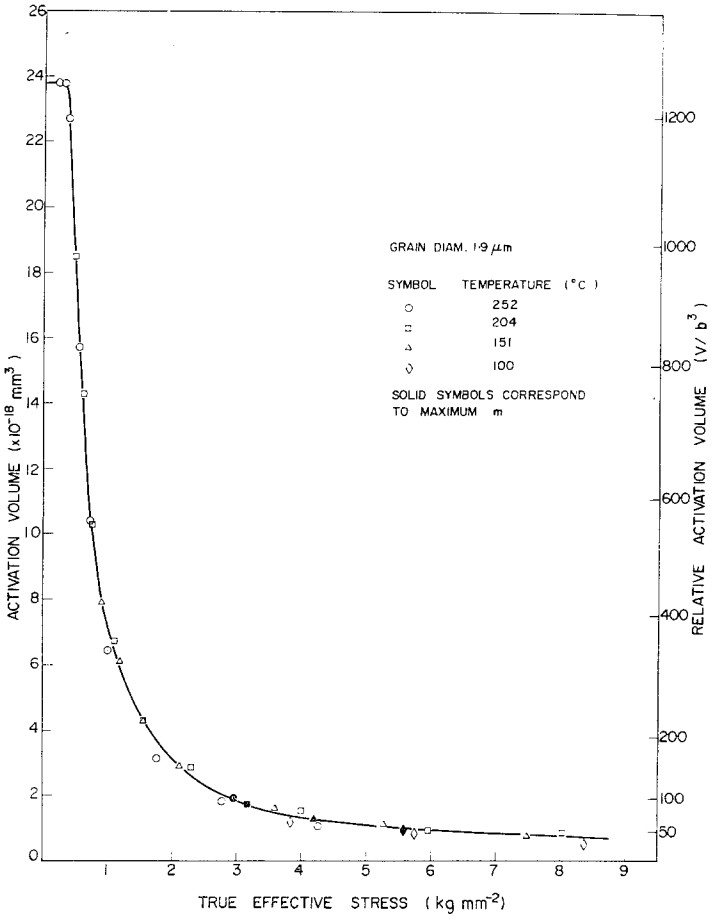

Figure 7 The true effective stress and grain diameter dependence of the activation volume at 204°C.

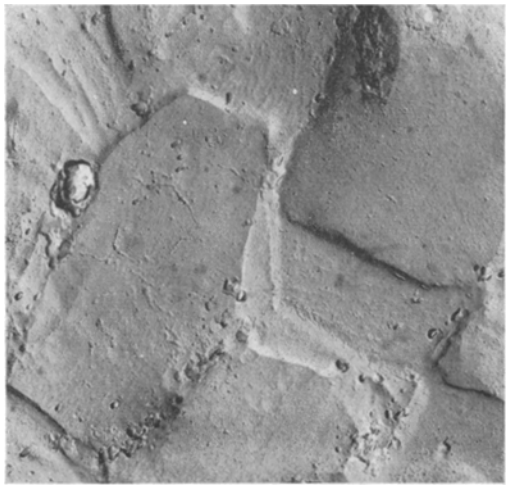

Figure 8 Carbon replica, showing the preferentially etched zones at tensile boundaries. Tensile axis approximately vertical. × 9700.

apparent grain elongation strain of 10%. This apparent strain was subtracted from ϵ_g to obtain the grain elongation due to deformation.

By comparing the transverse grain diameter W of deformed specimens with the initial transverse grain diameter W_0, it is possible to obtain a measure of grain growth during straining. Both the grain growth and grain elongation strain are shown in Fig. 11, for a temperature of 204°C and a mean strain-rate of 0.295 min^{-1}. The grain elongation in this case is approximately 17.5% of the applied strain. A similar halo effect has previously been observed by Karim *et al.* [8] and attributed to solute redistribution through diffusional creep. Solute redistribution also seems to cause the present effect.

The halo regions are depressed in relief, indicating that they have a higher chemical activity during etching than the grain interior. This high reactivity implies that the halo has a

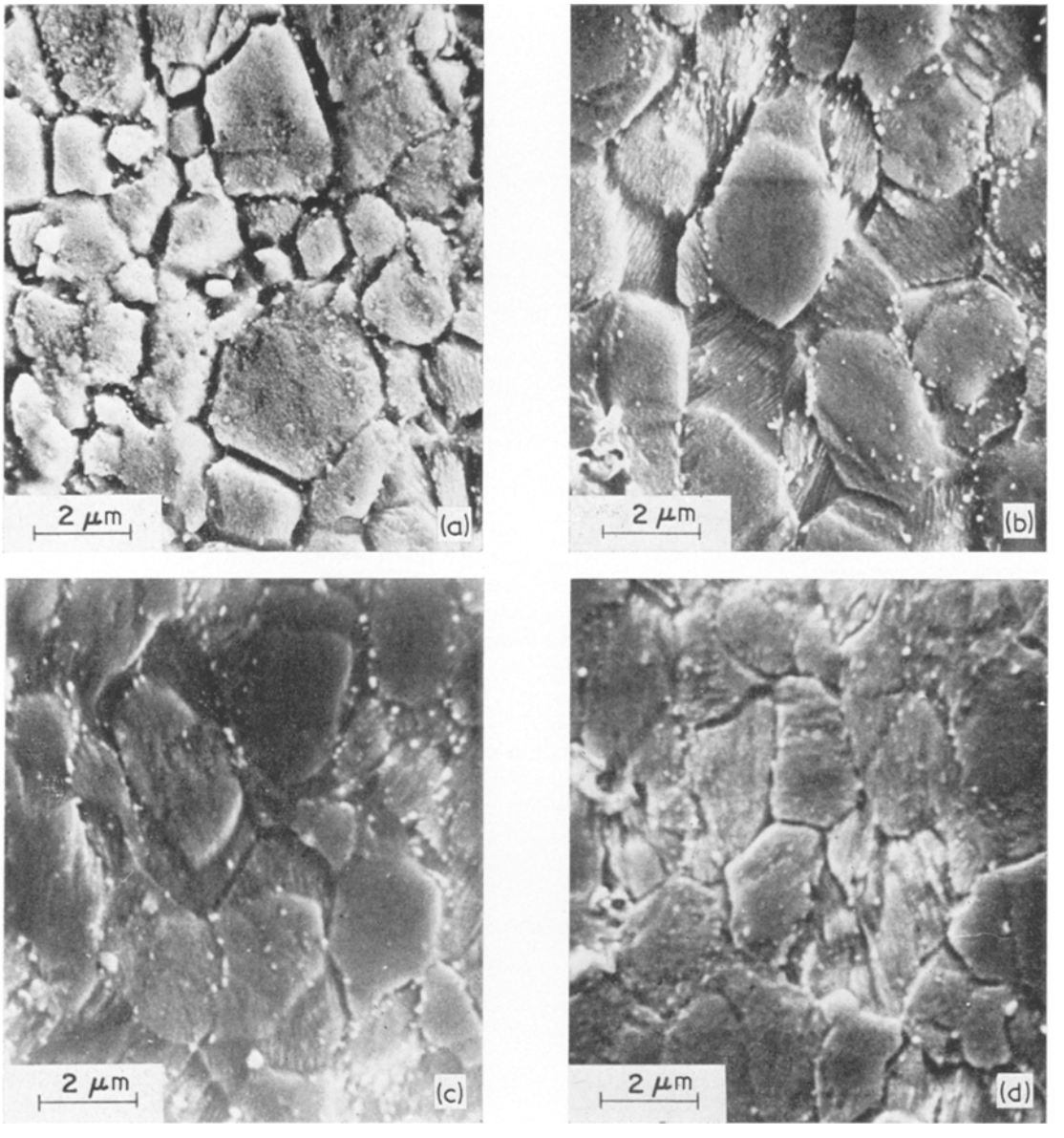

Figure 9 The effect of deformation at 204°C on the internal microstructure. Tensile axis vertical. (a) As-extruded; (b) $\dot{\epsilon}_m = 0.015\ min^{-1}$, $m = 0.37$; (c) $\dot{\epsilon}_m = 0.059\ min^{-1}$, $m = 0.49$; (d) $\dot{\epsilon}_m = 1.48\ min^{-1}$, $m = 0.36$.

different solute content than the rest of the grain. Of the three deformation mechanisms, Nabarro-Herring creep, Coble creep and dislocation glide, which could produce elongated grains only Nabarro-Herring and Coble creep could produce elongated grains only Nabarro-Herring and Coble creep could produce solute transfer. The material transported into the halo regions during diffusional creep will not have the same composition as the average composition of the alloy. The make-up of the atom flux will depend on the solute-vacancy binding energy. Magnesium and nickel have a distribution coefficient in zinc of less than one and will, according to Aust *et al.* [9] and van den Beukel [10], have a larger binding energy with vacancies than zinc. While it is easy to see that this difference in binding energy must lead to a different composition in the halo regions, it is not easy to decide, and impossible to show experi-

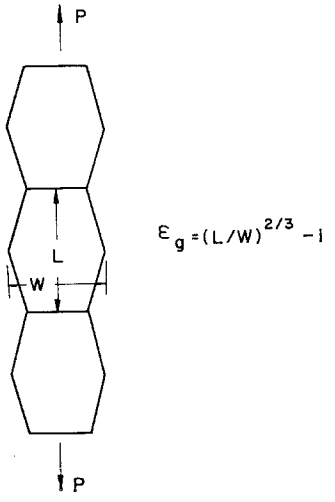

Figure 10 Calculation of the grain elongation strain. L = grain length parallel to the tensile axis. W = grain width perpendicular to the tensile axis. P = tensile load. ϵ_g = grain elongation strain.

mentally, whether these zones are enriched or impoverished in solute. This preferential etching of tensile regions will only be observed in alloys with low solute concentrations, like this zinc alloy, because in such alloys only a slight difference in composition between the base alloy and the atom flux will produce relatively large

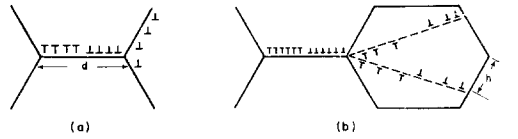

Figure 12 Cross-section of polycrystalline material (a) diffusion creep at grain-boundary triple points, (b) dislocation pile-up cascade [18].

concentration differences between the halo and the matrix.

Further confirmation that the halo effect was due to a solute redistribution effect was obtained after specimens which showed the strongest halo effect had been annealed for 1 h at 275°C. After re-polishing and etching no halos were observed.

3. Discussions

An effort was made to try to determine which of the two mechanisms, Nabarro-Herring or Coble creep, was contributing to the solute enriched zones. The equation relating the stress and strain rate for Nabarro-Herring creep [11, 12] is

$$\frac{\sigma}{\dot{\epsilon}} = \frac{d^2 kT}{\delta \lambda D_v} \tag{6}$$

where D_v is the volume diffusion coefficient of Zn, λ the atomic volume and δ a geometric constant ($\simeq$ 10).

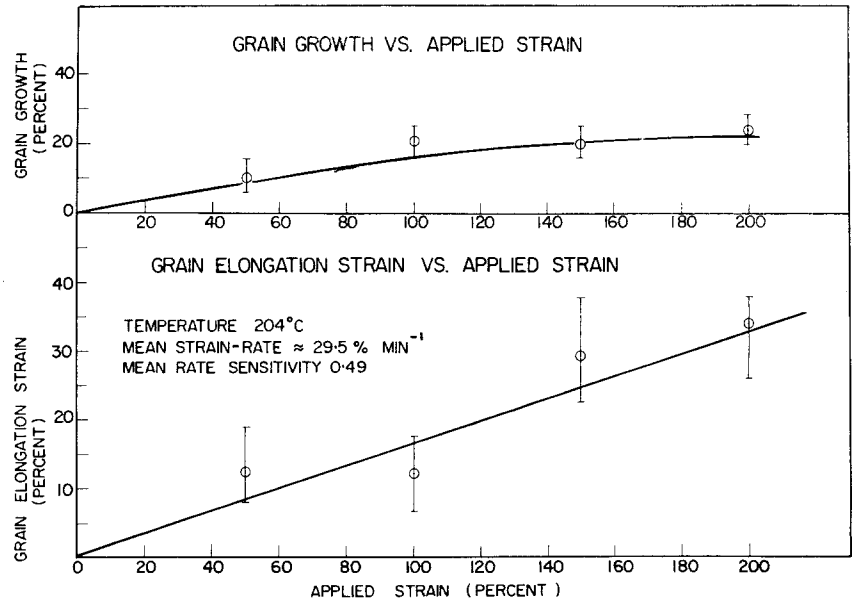

Figure 11 Grain elongation strain and grain growth as a function of the applied strain for an initial grain diameter of 1.9 μm at 204°C.

In the Coble analysis [13] of diffusional creep, the stress-strain rate relationship is:

$$\frac{\sigma}{\dot{\epsilon}} = \frac{\bar{d}^3 kT}{\phi \lambda w D_b} \tag{7}$$

where ϕ is a constant ($\approx$ 150), w the grain-boundary width and D_b the grain-boundary diffusion coefficient. Jones [14] has pointed out that grain-boundary diffusion should predominate for a given stress and temperature when

$$\frac{15w}{\bar{d}} D_b \gg D_v . \tag{8}$$

A comparison of the two quantities in Equation 8 at 204°C for the range of grain diameters studied indicated that grain-boundary diffusion was favoured by a factor of 12 to 48. (The smaller factor is associated with the largest grain size.) An activation energy for grain-boundary diffusion of 14.0 kcal mol^{-1} [15] and a grain width of 5 $\times$ 10^{-7} mm were used in this calculation. An activation energy of 22.7 kcal mol^{-1} for volume diffusion was taken from [16]. Coble creep appears to be the more favourable deformation mechanism for small grain sizes. However, the distinction between the two mechanisms decreases as the grain size increases.

The question which has yet to be answered is whether Coble creep could produce a significant strain for any the experimental strain-rates. In Table I the applied strain-rate and the Coble strain-rate (as calculated from Equation 8) are compared for the largest and smallest grain diameters tested. This rough calculation shows that Coble creep could certainly supply the necessary strain to produce elongated grains. It can also be seen from Table I that the direct strain contribution from Coble creep decreases as the strain-rate increases. This is in accord with Fig. 9 which shows an almost complete disappearance of the solute enriched zones at the highest strain-rate.

TABLE I Comparison of applied and Coble strain-rates for two grain diameters at 204°C

Grain diameter (μm)	Applied strain-rate (min^{-1})	Coble strain-rate (min^{-1})	Rate sensitivity (m)
1.9	7.60 $\times$ 10^{-3}	9.82 $\times$ 10^{-3}	0.32
1.9	1.72 $\times$ 10^{-1}	4.56 $\times$ 10^{-2}	0.51
7.4	9.56 $\times$ 10^{-4}	3.10 $\times$ 10^{-4}	0.47
7.4	7.03 $\times$ 10^{-2}	1.51 $\times$ 10^{-3}	0.24

Although the solute enriched zones and elongated grains at low strain-rates may be attributed to one of the diffusional creep mechanisms, neither of these deformation modes is consistent with a strain-rate sensitivity of less than one, nor do they explain the difference between the grain elongation strain and the imposed strain. Grain-boundary sliding could account for the difference between the two strains. Raj and Ashby [17] have shown that boundary sliding accommodated by boundary diffusion is described by an equation similar to Equation 7. However, this mechanism also has a strain-rate sensitivity of one when only diffusion provides the necessary accommodation for boundary sliding. Grain-boundary sliding, which is partially accommodated by dislocation glide, could account for a strain-rate sensitivity of less than 1.

There are, in the literature, a number of models which rationalize superplastic deformation behaviour on the basis of simultaneous diffusion and plastic flow processes. We shall base our further discussions on a recent model by Chaudhari [18]. This model suggests that in superplastic deformation grain-boundary sliding, grain-boundary diffusion and plastic flow occur simultaneously and that on the basis of this interaction of processes the high strain-rates at maximum m can be explained. He looks upon grain-boundary sliding as the movement of boundary dislocations involving a double pile-up as discussed by Hirth [19]. The necessary removal of material at boundary triple points is presented (Fig. 12a) as the climb of dislocations into the boundaries adjoining the triple point. For this process the boundary shear rate is

$$\dot{\epsilon}_g = \alpha \frac{D_b}{\bar{d}^3} \frac{\sigma_e \lambda}{kT} \tag{9}$$

where σ_e is now the stress field at the tip of the pile-up. It will be noted that this relation has the same form as Equation 7 for Coble creep, because both equations express that under these conditions, grain-boundary diffusion is the strain-rate controlling step. When the stress at the triple point exceeds a critical value, dislocations are generated in the grain through cascades of pile-ups from the triple point as shown in Fig. 12a). This enhances the rate of deformation through a reduction of the boundary climb distance from d to h. This change is reflected in an increased strain-rate and could qualitatively explain the sigmoidal stress/strain-rate relationship characteristic of many superplastic materials including the present.

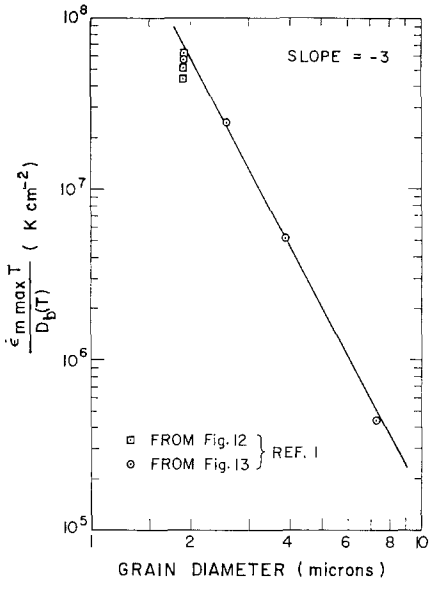

Figure 13 Plot of $\dot{\epsilon}_{m\max}T/D_b(T)$ versus grain size ($\bar{d}$) showing that $\dot{\epsilon}$ at maximum strain-rate sensitivity has a $\bar{d}^{-3}$ dependence.

Chaudhari shows that from this model the strain-rate, $\dot{\epsilon}_{m\max}$, at the peak of the strain-rate sensitivity is given by

$$\dot{\epsilon}_{m\ \max} = \frac{cD_b}{\bar{d}^3 T} \qquad (10)$$

In Fig. 13, $\dot{\epsilon}_{m\max}T/D_b(T)$ is plotted versus the mean grain diameter for this alloy. As indicated in that figure, $\dot{\epsilon}_{m\max}$ was taken from previous work on this alloy. For D_b the activation energy of 13.1 kcal g^{-1} at.$^{-1}$ was used which was shown to characterize the temperature dependence of the flow stress for this alloy over a large range of strain-rate sensitivity [1]. This value of activation energy is also very close to that measured for grain-boundary diffusion in pure zinc, namely, 14 kcal g^{-1} at.$^{-1}$ [15]. It is seen from Fig. 12 that $\dot{\epsilon}_{m\max}$ has an almost perfect $\bar{d}^{-3}$ dependence, indicating that rate controlling diffusion combined with plastic flow underlies the deformation of this alloy and that Chaudhari's model may very well be a close description of the interdependence of these processes. It should be noted that the observed constancy of activation energy of deformation over a range of strain-rates and its value very close to that of grain-boundary diffusion are in accord with that model.

The observed long range internal stress would qualitatively also fit this model. For this material, being essentially pure zinc, solute induced lattice distortion can certainly be ruled out as a source of an anelastic strain giving rise to negative flow at elevated temperatures. Because of the observed strong dependence of the internal stress (Fig. 2) on the grain size it is likely that both boundary adjustments and matrix flow lead to the anelastic effect. As the grain size increases, there will be fewer paths for grain-boundary sliding. Boundary segments which are not well oriented for sliding will be subjected to high stresses and stresses at triple points are high because of the large distances for boundary dislocation climb. The relaxation of dislocations flowing in response to these high stresses will produce negative creep. The temperature dependence of the internal stress (Fig. 2) would also fit this mechanism. At lower temperatures, where diffusive processes are slower, accommodation of dislocations into boundaries and the climb of dislocations in boundaries would be lower and consequently higher stresses exist.

Considering now the measured activation volumes, it is seen from Figs. 6 and 7 that all data derived at different temperatures and grain sizes can be incorporated into a single plot of activation volume versus effective stress. Increasing the strain-rate and grain size, or decreasing the temperature, shifts the system to a smaller activation volume. Also, it appears that for this superplastic alloy the activation volume decreases more rapidly with stress than is usually observed for coarse grained materials. It is also interesting to note that the maximum strain sensitivity occurs in the transition region between the area of rapidly changing activation volume with stress and one of much weaker stress dependence.

The activation volumes at maximum m are approximately 100 $\boldsymbol{b}^3$ where $\boldsymbol{b}$ is Burgers vector. Activation volumes of the same order of magnitude have also been observed in the superplastic deformation of a lead-cadmium alloy [20]. This indicates that over the range of effective stresses experienced by the material the activation volume-stress relationship reflects the glide of dislocations and the forces they encounter. If at any time during superplastic deformation the strain had been solely due to diffusive transport then an activation volume of approximately $\boldsymbol{b}^3$ should have been measured.

The activation volume dependence on stress, grain size and temperature is conceptually in complete agreement with a deformation mecha-

nism involving grain-boundary sliding, diffusive adjustments and plastic flow. However, from the present results it cannot be decided what relative contributions, boundary and bulk dislocations make to the negative creep, and whether or not the ratio of boundary relaxation to bulk relaxation changes with strain-rate and grain size. Possibly, long range internal stress measurements over a temperature range could provide an answer to the latter if a material can be found in which the temperature dependence of accommodation of dislocations into boundaries is known to be different from that of climb of boundary dislocations. One may expect that to be the case for some two-phase alloys.

Finally, without giving a mechanistic explanation why in this alloy the experimental activation volume decreases more rapidly with stress than is normally observed in coarse grained alloys, it can be shown that this observation is a consequence of the definition of activation energy and the rapidly changing stress sensitivity of fine grained materials. For infinitesimal stress changes the denominator of Equation 3 may be replaced by its mathematical equivalent $\partial\sigma_e = \sigma_e \partial \ln \sigma_e$, so that

$$\bar{V} = \left(\frac{kT}{N\sigma_e m}\right)_T \qquad (11)$$

where $\partial \ln \dot{\epsilon} / \partial \ln \sigma_e \doteq m^{-1}$ when the long range internal stress is small. Therefore, a fine grained metal, in which both σ_e and m increase with strain-rate will exhibit a smaller activation volume than a coarser grain material for which m is low and approximately constant.

4. Summary

In this dispersion strengthened zinc alloy both dislocation movement and diffusional creep appear to be operating simultaneously over a region where the strain-rate sensitivity increases with strain-rate. Since neither dislocation glide nor diffusional creep appear to make a large contribution to the total strain, it is suggested that these mechanisms operate to promote grain-boundary sliding.

A long range internal stress has been observed after deformation. The internal stress increases with strain-rate and represents 20 to 35 % of the applied stress at a strain-rate of 10^{-3} min^{-1}. All data derived at different temperatures and grain sizes can be incorporated into a single plot of activation volume versus effective stress. Increasing the strain-rate and grain size, or decreasing the temperature shifted the system to a smaller activation volume.

Regions of different solute concentration at tensile grain boundaries suggest that diffusional creep operates over the range where the rate sensitivity increases with strain-rate. From calculations it is shown that, for the small grain sizes and low strain-rates, Coble creep is the predominant deformation mechanism. The strain-rate at maximum strain-rate sensitivity has a (grain size)$^{-3}$ dependence as suggested in a recent model in which grain-boundary sliding, grain-boundary diffusion and plastic flow occur simultaneously during superplastic deformation. The obtained results fit this model, at least qualitatively, in all respects.

Acknowledgements

This work was supported by the National Research Council of Canada. We also wish to thank the Product Research Centre of COMINCO for the donation of high purity zinc and the casting and extrusion of alloy rods.

References

1. J. D. LEE and P. NIESSEN, *Met. Trans.* **4** (1973) 949.
2. J. E. HILLIARD, *Metal Progress*, May (1964) 99.
3. G. B. GIBBS, *Phil. Mag.* **13** (1966) 317.
4. *Idem, Phys. Stat. Sol.* **5** (1964) 693.
5. F. GUIU and P. L. PRATT, *Phys. Stat. Sol.* **6** (1964) 111.
6. N. BALASUBRAMANIAN and J. C. M. LI, *J. Mater. Sci.* **5** (1970) 434.
7. W. A. RACHINGER, *J. Inst. Metals* **81** (1952-53) 33.
8. A. KARIM, D. L. HOLT and W. A. BACKOFEN, *Trans. Met. Soc. AIME* **245** (1969) 1131.
9. K. T. AUST, R. E. HANNEMAN, P. NIESSEN and J. WESTBROOK, *Acta Met.* **16** (1968) 291.
10. A. VAN DEN BEUKEL, *Phys. Stat. Sol.* **23** (1967) 165.
11. F. R. N. NABARRO, Proceedings of the Conference on Strength of Solids, (Phys. Soc. of London, Cambridge, 1948) p. 75.
12. C. HERRING, *J. Appl. Phys.* **21** (1950) 437.
13. R. L. COBLE, *ibid* **34** (1963) 1679.
14. R. B. JONES, *Nature* **207** (1965) 70.
15. E. S. WADJA, *Acta Met.* **2** (1954) 184.
16. J. ASKILL, "Tracer Diffusion Data for Metals, Alloys and Simple Oxides" (IFI/Plenum, New York, 1970).
17. R. RAJ and M. F. ASHBY, *Met. Trans.* **2** (1971) 1113.
18. P. CHAUDHARI, *Met. Trans.* **5** (1974) 1692.
19. J. P. HIRTH, *Met. Trans.* **3** (1972) 3047.
20. P. CHAUDHARI and S. MADER, Proceedings of the 7th International Symposium on High Speed Testing: The Rheology of Solids, Boston (1969); *J. Appl. Polymer Sci.* **12** (1969).

Received 6 December 1973 and accepted 3 April 1974.